LANGMUIR Article
Cite This: Langmuir 2018, 34, 585−594
pubs.acs.org/Langmuir

Growth of Sub-5 nm Metal Nanoclusters in Polymer Melt Aerosol Droplets

Yong Yang, Michelangelo Romano, Guangjie Feng, Xizheng Wang, Tao Wu, Scott Holdren, and Michael R. Zachariah*

University of Maryland, College Park, Maryland 20742, United States

Supporting Information

ABSTRACT: Ultrasmall metal nanoparticles are inherently unstable because of their high specific surface area. This work investigates how growth and aggregation of these nanostructures can be circumvented by incorporating them into a polymer matrix in an on-the-fly growth process. We demonstrate the formation of sub-5 nm particles of Ni, Co, and Cu nanoparticles in a polymer matrix using an aerosol single-drop reactor approach. The rapid thermal pulse given to the aerosol particles enables the formation of nuclei and growth, with subsequent rapid quenching to freeze in the structure. The role of the temperature as well as the precursor concentration of the resulting size and morphology is discussed. A characteristic time analysis and an analysis of the particle size distributions lead to the conclusion that growth is governed by nucleation and surface growth, with little coagulation or Ostwald ripening. Finally, we note that this aerosol route is amenable to scale-up for large-scale production of nanoclusters that can either be used as is within the polymer or released by solvent extraction, depending on the application.

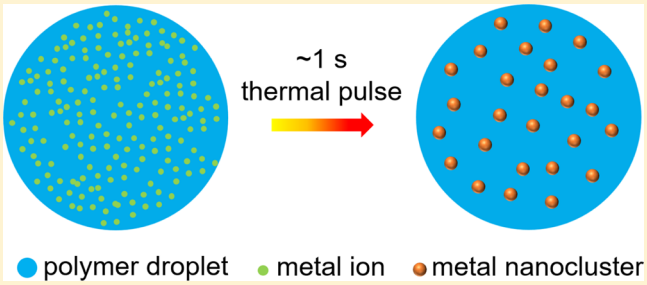

1. INTRODUCTION

Ultrasmall metal nanoparticles with a diameter less than 5 nm have been of great interest in recent years because of their unique size- and shape-dependent properties, enabling applications in the fields of plasmonics, photonics, catalyst, nanomedicine, and magnetic storage, among others.[1−5] Synthesizing these extremely small nanoparticles, at least in sufficient quantities to enable their utility, is challenging because of their high mobility and meta-stable nature, which results in aggregates or particle growth. One approach to potentially overcome this challenge is by encapsulating the nanoparticles within a polymer matrix so that these nanoparticles are physically frozen in the polymer matrix or chemically stabilized via forming covalent bonds with polymer molecules, ultimately preventing nanoparticle agglomeration and oxidation.[6−8]

These hybrid materials are referred to as metal−polymer nanocomposites. Fundamentally, the polymer serves as a framework for stabilizing nanoparticles. However, the strategic combination of nanoparticles and specific types of polymers can yield enhanced functionality for these composite materials.[9] In many cases, nanoparticles incorporated within polymers have been demonstrated to increase the system's mechanical stability.[10,11] Other synergistic effects have augmented the composite material's electrical and optical properties. For example, the introduction of metal nanoparticles into organic photovoltaics has led to improved efficiencies, stemming from the enhanced light absorption and scattering properties of the incorporated nanoparticles.[12] Furthermore, nanoparticles embedded within electrically conductive polymers have the potential to serve as innovative composite materials for electrodes within Li-ion batteries.[13]

Synthesis of metal−polymer nanocomposites has been accomplished by both ex situ and in situ composite stabilizations. In ex situ stabilization, metal nanoparticles are first synthesized by processes such as colloidal chemistry, nanolithography, laser ablation, sputtering, and ball-milling and subsequently introduced within a polymer matrix.[8,14] One major difficulty in this approach is homogeneous incorporation of nanoparticles into the polymer matrix and the prevention of aggregation. Alternatively, in situ techniques refer to the formation of nanoparticles directly within a polymer matrix. This fabrication method first incorporates metal-ion precursors into a polymer matrix, from which nanoparticles are generated in the polymer matrix via thermal reduction or decomposition of metal-ion precursors.[15−20] In essence, the polymer functions as a soft template for guiding the nucleation and growth of the metal nanoparticles. This method eliminates the need for surfactants and capping agents, yielding a higher nanoparticle number density and more uniform nanoparticle distribution throughout the polymer matrix. However, most in situ and ex situ techniques reported in the literature typically generate metal−polymer nanocomposites in small quantities. The difficulty lies in increasing the production rate which, for a

Received: September 6, 2017
Revised: December 16, 2017
Published: December 17, 2017

DOI: 10.1021/acs.langmuir.7b02900
Langmuir 2018, 34, 585−594

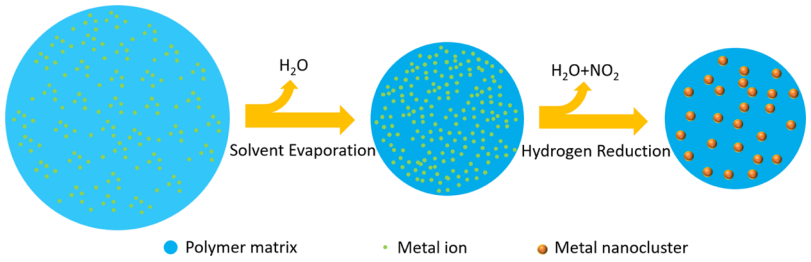

Figure 1. Schematic of the formation of nanoclusters in an aerosol polymer droplet.

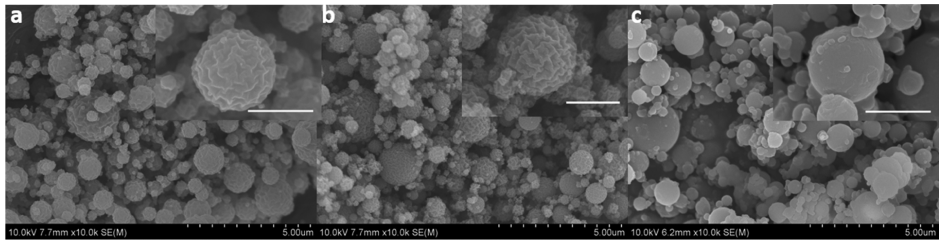

Figure 2. SEM images of metal–polymer nanocomposites. (a) Ni PVP8k, (b) Co PVP58k, and (c) Cu PVP8k. The length of the scale bar in the inset images is 1 μm.

bulk system, typically involves inhomogeneous and slow heating and cooling rates. This typically leads to wide size distribution, inhomogeneous dispersion, and aggregation.[21]

Ideally, one would like to control the thermal pulse to trigger chemistry over a short time scale and do so homogeneously. One approach to accomplish this is to conduct the synthesis within an aerosol particle and use inherent rapid thermal equilibration of the particle to ensure precise control and homogeneous heating. Further, because of the small thermal mass, heating and cooling can be rapid, and achieving higher temperatures for shorter duration is possible. Because such a process is continuous, scaling becomes greatly simplified. Aerosol routes such as aerosol spray pyrolysis (ASP) have been used to generate nanoparticles and nanocomposites.[21−23] In a typical ASP process, the precursor solution is continuously nebulized to produce aerosol droplets from hundred nanometers to several micrometers in diameter, and these aerosol droplets, acting like small isolated reactors, pass through a heating element where the reaction in each aerosol reactor is triggered by a short thermal pulse to generate nanostructured materials upon solvent evaporation. Although the ASP technique has been used to produce and assemble a large range of materials (metals,[24] alloys,[25] metal oxide,[26−28] and composites[29−31]) with controllable size and morphologies, fabrication of nanoparticles with a diameter of sub-50 nm, which is much smaller than that of the nebulized aerosol droplets, using this technique remains challenging. Recently, efforts have been made to produce small and monodisperse nanoparticles by introducing an inert solute into the aerosol droplets to guide the nucleation and growth of nanoparticles.[32,33] For example, Xia et al. have introduced sodium chloride into the precursor solution to guide the formation of sub-10 nm NiO and ZnS nanoparticles.[32] Few studies have been reported on using this technique to synthesize metal–polymer nanocomposites. One primary exception is Lee et al. who embedded silver nanoparticles in a polyvinylpyrrolidone (PVP) matrix by thermal decomposition of silver nitrate.[34] However, encapsulation of nonnoble metals cannot be achieved via this approach because thermal decomposition of salts of reactive metals would produce metal oxides. Seo et al. incorporated copper nanoparticles with diameters ranging from 30 to 50 nm in the PVP matrix by reducing copper nitrate with ethanol as a reducing agent.[35]

In this paper, our focus is the synthesis of high density unaggregated ultrasmall nanoparticles of zero-valent metals with a very narrow size distribution. To our knowledge, this is the first demonstration of the formation of sub-5 nm metal nanoparticles (e.g., Ni, Co, and Cu) incorporated into polymer particles (~several hundred nanometers to 1.5 μm) in a one-step ASP process. We demonstrate that this is a generic facile process to produce virtually any metallic nanoparticle and evaluate the role of temperature and metal precursor loading on particle properties.

2. EXPERIMENTAL SECTION

2.1. Materials. Nickel nitrate hexahydrate ($Ni(NO_3)_2{\cdot}6H_2O$, ≥99% pure), copper nitrate trihydrate ($Cu(NO_3)_2{\cdot}3H_2O$, ≥99% pure), and cobalt nitrate hexahydrate ($Co(NO_3)_2{\cdot}6H_2O$, ≥98% pure) were all purchased from Sigma-Aldrich. PVP powders with three different molecular weights (MW 1 300 000; 58 000; and 8000 g/mol) were obtained from Alfa Aesar. All the chemicals were used as received.

2.2. Precursor Preparation. The precursor solutions were prepared by dissolving 425 mg of the PVP polymer and a certain amount of metal salt in 25 ml of deionized water. The metal salts used to obtain Ni, Co, and Cu nanoparticles were $Ni(NO_3)_2{\cdot}6H_2O$, $Co(NO_3)_2{\cdot}6H_2O$, and $Cu(NO_3)_2{\cdot}3H_2O$, respectively. The mass of the metal salt used was varied between 42.5 and 425 mg to prepare precursor solutions with different metal salt precursor to polymer mass ratios (0.1, 0.3, 0.5, and 1.0).

2.3. Aerosol Spray Pyrolysis. Aerosol droplets containing metal salts and polymer molecules with a desired mass ratio were created from a pneumatic collision nebulizer with a 5% hydrogen and 95% nitrogen mixture as the carrier gas. Figure 1 shows schematically the basic concept behind the synthesis scheme. Most of the water solvent is removed from the droplets as they pass through a silica gel diffusion dryer, from where they are carried to a tubular furnace (28 cm in length and 2 cm in diameter) for a residence time of ~1 s. The set temperature of the tube furnace was varied from 400 to 800 °C. Within the heated flow, the dried polymer particles are molten, and the metal salt is decomposed and reduced in H_2 to form metal nanoparticles in the polymer melt. Rapid quenching on a 0.4 μm

DOI: 10.1021/acs.langmuir.7b02900
Langmuir 2018, 34, 585−594

Table 1. Synthetic Conditions for Spray Pyrolysis

nanocomposite	metal salt	PVP molecular weight (g/mol)	metal salt to PVP ratio	pyrolysis temperature (°C)	residence time (s)
Ni PVP8k	$Ni(NO_3)_2{\cdot}6H_2O$	8000	1.0	600	1
Co PVP58k	$Co(NO_3)_2{\cdot}6H_2O$	58 000	1.0	700	1
Cu PVP8k	$Cu(NO_3)_2{\cdot}3H_2O$	8000	0.3s	600	1

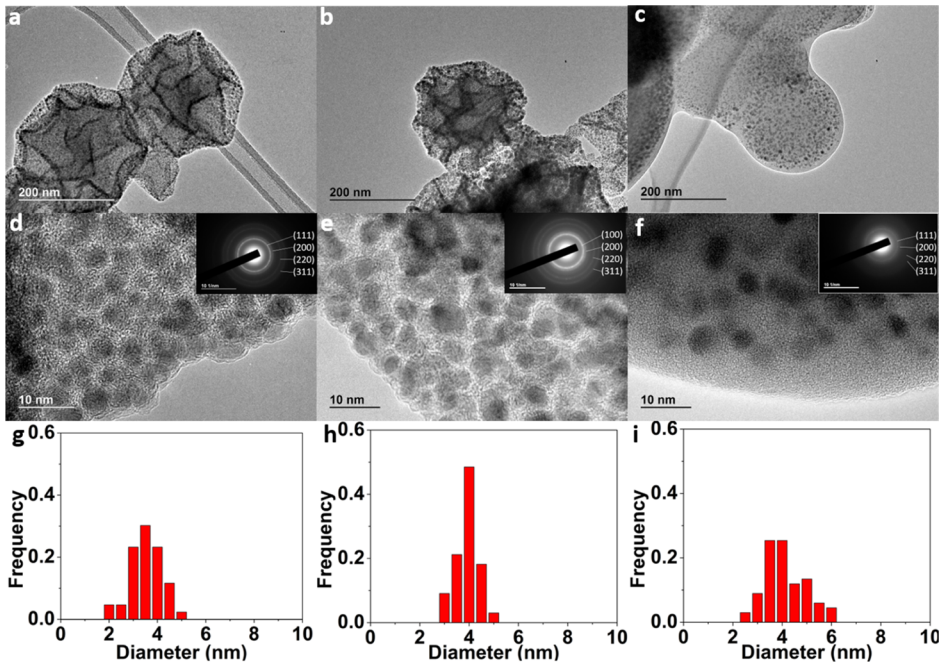

Figure 3. TEM images and metal nanocluster size distributions in metal−polymer nanocomposites. (a,d,g) Ni PVP8k; (b,e,h) Co PVP58k; and (c,f,i) Cu PVP8k.

pore Millipore HTTP membrane filter results in arresting of nanoparticle growth.

2.4. Characterization. Morphologies and structures of metal−polymer nanocomposites were examined by scanning electron microscopy (SEM, Hitachi SU-70) and transmission electron microscopy (TEM, JEOL JEM 2100 FEG). Elemental distribution in the nanocomposite particle was analyzed by energy-dispersive X-ray spectroscopy (EDS) mapping on TEM. The mean diameters and size distributions of the nanoparticles were determined by statistical analysis of the acquired TEM images using Nano Measurer 1.2 image analysis software.[36] Phase and component identification was conducted by an X-ray diffractometer (Bruker D8 diffractometer with Cu Kα radiation). The structure of the polymer molecules was characterized by Fourier transform infrared spectroscopy (FTIR). Thermogravimetric analysis (TGA) of the PVP polymer was carried out using a thermogravimetric analyzer (TA Instruments, USA) with a heating rate of 10 °C/min in argon gas.

3. RESULTS AND DISCUSSION

3.1. Formation of Metal−Polymer Nanocomposites. Figure 2 shows SEM images of metal−polymer nanocomposites containing Ni, Co, and Cu nanoparticles. Information about the precursor solutions and operation parameters used to generate these three types of nanocomposites is summarized in Table 1. As shown in Figure 2, all three nanocomposites have a spherical shape with a size distribution roughly ranging from several hundred nanometers to 1.5 μm. In particular, Ni and Co polymer nanocomposites shown in Figure 2a,b have a crumpled surface morphology. Similar surface morphologies have also been observed by others who have synthesized composite materials using the precursor containing polymer molecules and metal salts by the ASP technique.[29,35] Although we have no definitive conclusion about how the crumpled surface was formed, it may be related to the gas release during hydrogen reduction of metal nitrate (eq 1, M represents metal element) in the presence of the high viscous polymer melt. Surface corrugation of the polymer particles appears to scale closely with the metal salt to PVP ratio. For example, Figure 2c shows Cu polymer nanocomposites formed using a much lower metal salt to PVP ratio (0.3) compared to the polymer nanocomposites in Figure 2a,b (1.0). The lower metal salt to PVP ratio formulation created particles with a smoother surface.

$$M(NO_3)_2 + 2H_2 \rightarrow M + 2NO_2 \uparrow + 2H_2O\uparrow \quad (1)$$

Slow-heating TGA data of PVP shown in Figure S1 demonstrate that PVP molecules are fully decomposed at temperatures above 460 °C. However, aerosolized PVP particles which were actually heated to much higher temperatures appear to survive because of their very short residence time in the reactor (~1 s.). FTIR analysis of 600 °C spray-pyrolyzed PVP particles (of different molecular weights) showed no discernable evidence of polymer degradation (see Figure S2). PVP sample powders were also characterized by SEM. The sprayed PVP powders have a spherical shape with a smooth surface morphology, as shown in Figure S3. However, despite the lack of any spectroscopic evidence for polymer chemistry under such short heating, we did notice that spray-pyrolyzed 1300k PVP was more easily dissolved in water compared to the commercial reagent PVP, suggesting the possibility of polymer cleavage, leading to a lower average molecular weight after short heat shock.

DOI: 10.1021/acs.langmuir.7b02900
Langmuir 2018, 34, 585−594

The X-ray diffraction (XRD) patterns of the three metal−polymer nanocomposite powders are shown in Figure S4. The broad and flat peak located at around 20° on each XRD pattern belongs to the PVP matrix. It was observed that nickel and copper nitrate were completely reduced to metallic nickel and copper by hydrogen gas at a reaction temperature of 600 °C with a resident time of 1 s. However, metallic cobalt was only obtained at a reaction temperature of 700 °C. These results are consistent with other studies on fabricating pure metal powders by hydrogen reduction of metal salts via ASP with similar operating conditions.[24,37−39] To test the stability of the metal nanoparticle incorporated in the PVP matrix, the Ni polymer nanocomposite was exposed to air for >1 month, and the metallic nickel phase was still observed by XRD (see Figure S4). This suggests that the PVP matrix is able to protect metal nanoparticles from oxidation.

The size and distribution of metal nanoparticles (Ni, Co, and Cu) dispersed in polymer matrices were characterized by TEM, as shown in Figure 3 (see also Figure S5 for scanning TEM and EDS mapping characterization). The three selected-area electron diffraction patterns (insets of Figure 3) confirm the presence of pure Ni, Co, and Cu metals, which indicates that Ni, Co, and Cu ions have been reduced to their metallic states by H_2. This result is consistent with the aforementioned XRD data. As shown in Figure 3, monodispersed Ni, Co, and Cu nanoparticles with an average diameter of 3.5, 3.9, and 4.1 nm, respectively, are uniformly distributed in the polymer particles. The size difference between the different metal nanoparticles may be attributed to both different mass fractions of metal nanoparticles in the polymer matrix and various interactions between different metal nanoparticles and polymer molecules. With the full conversion of metal salts to metal elements and the complete release of other byproducts such as water vapor and NO_2 from the polymer particles, the total mass and volume fractions of the metal nanoparticles can be derived based on the metal salt to PVP ratio used to prepare the precursor solutions. The calculated total mass fractions of metal nanoparticles are listed in Table S1. Table S1 also includes the areal number concentrations and number-average diameter of the metal nanoparticles obtained by statistical analysis of metal nanoparticles in TEM images. The areal number concentration was calculated based on the number of particles divided by the corresponding nanocomposite particle area in TEM images. As shown in Table S1, both mass fractions of Ni and Co metals in polymer matrices are around 16.8%. The formed Ni and Co nanoparticles have similar areal concentrations and diameters. This aligns well with our findings that the metal nanoparticle diameter increases with the metal salt concentration (discussed in more detail in section 3.3). However, the generated Cu nanoparticles also have a similar diameter compared to Ni and Co nanoparticles even though a much lower mass fraction (7.9%) of copper was loaded in the PVP matrix. This suggests that besides the mass loading of metal salts, additional factors also affect the particle size. Previous studies have shown that stronger polymer−nanoparticle surface interactions enabled the formation of smaller nanoparticles[40] and that the strength of the interaction between the polymer matrix and metal nanoparticles are related to the reactivity of the metal.[41] We conclude that Cu−polymer interactions will be weaker compared to the Ni− or Co−polymer interactions because Cu is less reactive. These weaker interactions allow Cu to form larger nanoparticles with a lower mass loading. As a result, Cu nanoparticles with a similar diameter compared to Ni and Co nanoparticles were synthesized even though a lower mass fraction between the metal and PVP was used in the precursor solution.

In the following, the Ni−polymer nanocomposite system is used to demonstrate how the temperature and metal salt to polymer ratio affect nucleation and growth.

3.2. Effect of Temperature on the Size and Phase Evolution of Metal Nanoparticles. The precursor solutions composed of nickel nitrate salt and PVP8k with a mass ratio of 1.0 were spray-pyrolyzed at different temperatures. It is known that under slow heating (0.6 °C/min) and in the presence of H_2, nickel nitrate converts to metallic nickel at 270 °C.[42] However, figure 4 shows that at fast heating (short residence times), metallic nickel is only seen at temperatures of 600 °C or above.

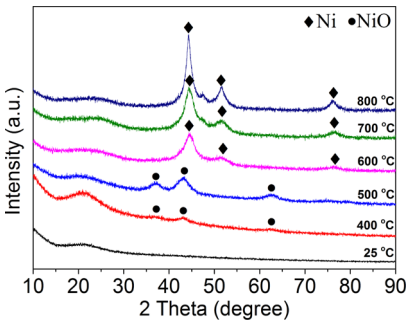

Figure 4. XRD of metal−polymer nanocomposite synthesis under various reaction temperatures.

The effect of reaction temperature from 400 to 800 °C on the morphology of the metal−polymer nanocomposite and the growth of Ni nanoparticles in the polymer matrix is shown in Figure 5. The mass ratio between nickel nitrate and polymer in precursor solutions was maintained at 0.3. At 600 °C and above, a crumpled surface morphology is observed, presumably caused by gas release during a reduction reaction of the metal nitrate in the polymer melt. However, no crumpled texture was observed on the surface of the products produced at temperatures of 500 °C and below, where the conversion to Ni nanoparticles was not complete. This is confirmed by the observation that the volume fraction of the nanoparticles formed at 500 °C (Figure 5g) is smaller than that of the nanoparticles formed at 600 °C (Figure 5h).

From the TEM images shown in Figure 5, NiO nuclei with a diameter of less than 1 nm were formed at around 400 °C and grew to larger NiO nanoparticles with an average diameter of 1.5 nm at 500 °C. The ultrasmall unaggregated Ni nanoparticles with an average diameter of 2.3 nm were generated at 600 °C. This result indicates that intradrop coagulation (the process in which single particles diffuse together to form an agglomerate) is slow for the given residence time (~1 s). However, as seen in Figure 5i,j, aggregation between nanoparticles is observed at higher reaction temperatures of 700 and 800 °C. This is consistent with high temperatures, facilitating the diffusion of particles in the polymer melt and a likely decrease in the polymer−metal interaction energy.[43] The coagulation between nanoparticles leads to a decrease in the number concentration of the Ni nanoparticles in the temperature range from 700 to 800 °C, as shown in Figure 6. The fact that the agglomerates are seen at all (primary particles 2−3 nm) indicates that coalescence (the process in which an agglomerate

DOI: 10.1021/acs.langmuir.7b02900
Langmuir 2018, 34, 585−594

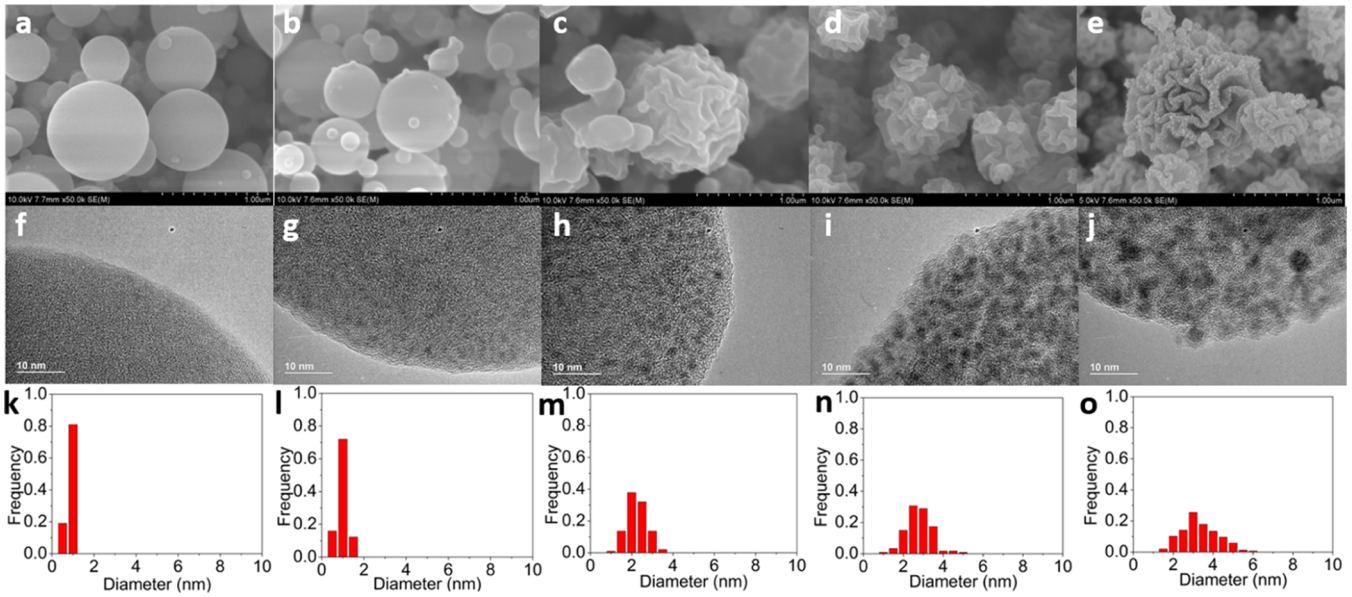

Figure 5. SEM and TEM images of Ni/NiO polymer nanocomposites synthesized at different reaction temperatures. (a,f,k) 400, (b,g,l) 500, (c,h,m) 600, (d,i,n) 700, and (e,j,o) 800 °C.

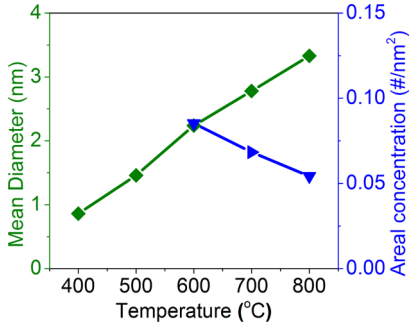

Figure 6. Size and number concentration evolution of Ni/NiO nanoparticles with reaction temperature.

sinters together to gain a spherical morphology) is slow compared to the residence time. Results in Figure 6 show that the average size monotonically scales with the reaction temperature at a fixed residence time. This result clearly demonstrates that the use of a polymer encapsulant can be used as a reaction medium at temperatures well above its decomposition temperature, for short thermal pulses, enabling the nucleation, growth, and stabilization of metal ultrafine nanoclusters.

3.3. Effect of Mass Loading on the Size of Metal Nanoparticles. By simply adjusting the mass of the metal salt in the ASP precursor, the metal salt to polymer ratio in the sprayed droplet can be adjusted. The SEM images in Figure 7a–d show that the morphology of the nanocomposites changed with the metal salt to PVP ratio. The crumpled surface

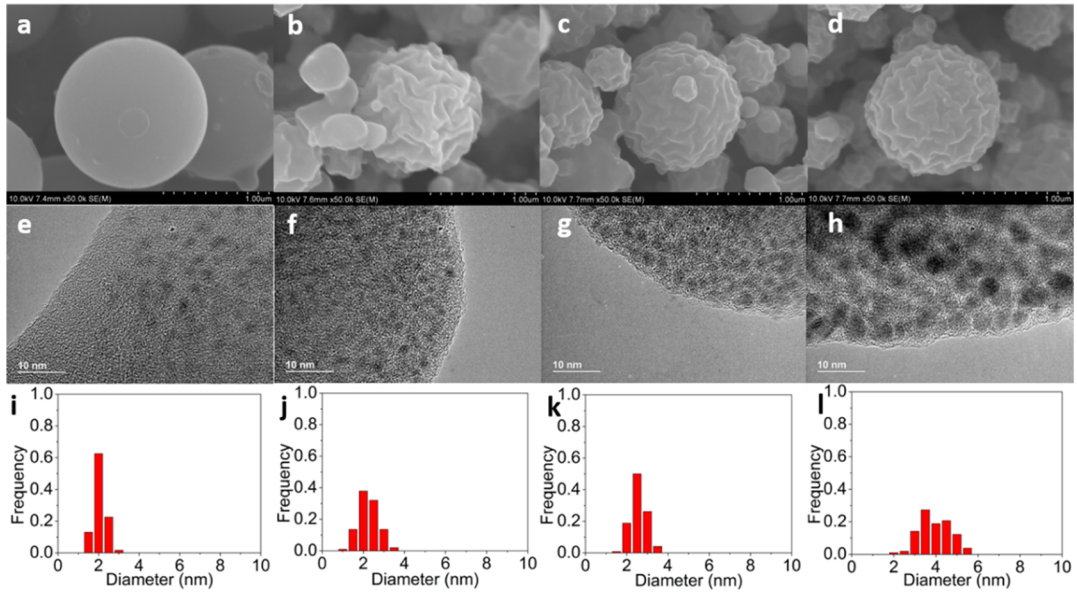

Figure 7. SEM and TEM images of metal–polymer nanocomposites with different metal salt to PVP ratios. (a,e,i) 0.1, (b,f,j) 0.3, (c,g,k) 0.5, and (d,h,l) 1.0.

DOI: 10.1021/acs.langmuir.7b02900
Langmuir 2018, 34, 585–594

morphology is observed primarily for high mass metal salt loading samples because of the mass loss through gas release from the reduction reaction of nickel nitrate salt. Figure 7e–i shows the TEM micrographs and size distribution histograms of Ni nanoparticles synthesized with varying the metal salt to polymer ratio. Clearly, increasing the ratio yields larger particles in the polymer matrix. Interestingly, for all metal salt to polymer ratios investigated in this study, unaggregated and uniform nanoparticles were generated at a reaction temperature of 600 °C. The trends of the average diameter and the areal number concentration of Ni nanoparticles as a function of metal salt to polymer ratio are presented in Figure 8. The areal

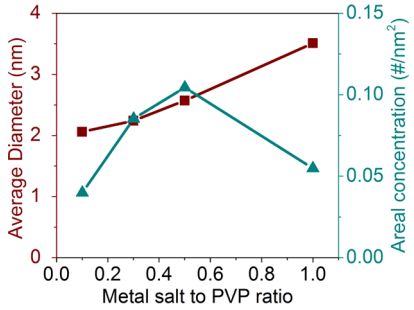

Figure 8. Average diameter and areal concentration of Ni nanoparticles as a function of the metal salt to polymer ratio.

concentration increases initially with the metal salt to polymer ratio (0 < ratio < 0.5), but at higher loadings, (0.5 < ratio < 1) the nanoparticle concentration in the polymer matrix is observed to decrease.

The most noticeable effects we observed from the metal salt loading are the consistent formation of unaggregated, relatively monodisperse particles and the change in the areal concentration. First, the formation of unaggregated, relatively monodisperse particles suggests that intradroplet coagulation is slow for the given residence time of ∼1 s. A more detailed discussion of the mechanism and particle distribution will occur later in this paper. Second, as seen in Figure 8, the size scales with the precursor concentration (0 < ratio < 0.5). This suggests that after the nucleation burst, metal atom diffusion and surface growth dominate. Third, the concentration peaks at a mass loading ratio of 0.5 decrease, as shown in Figure 8. This suggests that highly concentrated nuclei are formed to enable coagulation and coalescence at the early state of nanoparticle formation. However, coagulation and/or coalescence cannot be a dominant growth mechanism at the late stage of nanoparticle formation. Otherwise, monodisperse nanoparticles should not be observed as shown in Figure 7h.

3.4. Dynamics of Nanoparticle Growth in a Polymer Melt. The nucleation and growth mechanisms of nanoparticles in small molecule solvents have been extensively studied for the past two decades.[44,45] However, only a few studies have focused on the formation mechanism of nanoparticles in a polymer melt.[43,46] The experimental results in this study show that the number concentration of metal nanoparticles decreases with increasing reaction temperature or metal salt to PVP ratio (0.5 < ratio < 1). This result suggests that pure surface growth (simple monomer attachment) might not be the only factor controlling the growth process. Two additional pathways for growth include Ostwald ripening and coagulation, both of which can lead to a decrease in the concentration.

The diffusivity of the nanoparticles in a polymer melt can be estimated by the Stokes–Einstein equation[47]

$$D = \frac{k_B T}{3\pi\eta d_p} \tag{2}$$

where k_B is the Boltzmann constant, T is the absolute temperature, d_p is the particle's diameter, and η is the viscosity of the polymer.[48] The viscosity of PVP 8k over a temperature range from 140 to 185 °C has previously been measured.[49] The viscosity at the high temperature region (up to 800 °C) was predicted by fitting and extrapolating the aforementioned experimental data[49] using the Masuko and Magill model,[50] which is shown in Figure S6. Figure S7 shows the calculated diffusion coefficient of Ni nanoparticles as a function of diameter in the polymer melt at 600 °C.

To understand the dynamic behavior of nanoparticles in the polymer melt, the characteristic coagulation and coalescence times were estimated and compared to the residence time of the aerosol droplets. The characteristic coagulation time is defined as the time required for the nanoparticles with an initial concentration of N_0 to achieve half of the initial concentration. The continuum Brownian coagulation coefficient is given in eq 3[51]

$$K_{12} = 2\pi(D_1 + D_2)(d_{p1} + d_{p2}) \tag{3}$$

where D_1 and D_2 are the diffusion coefficients for nanoparticles with a diameter of d_{p1} and d_{p2}, respectively. For nanoparticles with a narrow size distribution, such as what we observe, eq 3 becomes

$$K = 8\pi D d_p = \frac{8k_B T}{3\eta} \tag{4}$$

where D is the diffusivity of the nanoparticles shown in eq 2. Equation 4 indicates that the coagulation coefficient K is independent of the diameter for monodispersed nanoparticles.

The characteristic coagulation time can then be written as[51]

$$\tau_c = \frac{2}{KN_0} \tag{5}$$

where N_0 is the number concentration of nanoparticles in a polymer droplet. For samples with a constant metal salt to polymer ratio (0.3 is used for calculation), $N_0 \propto 1/d_p^3$ (d_p is the diameter of the Ni nanoparticles) based on the mass conservation of the nickel component in the polymer droplet.

The characteristic coalescence time for Ni nanoparticles was also estimated. The characteristic coalescence time is the time required for two contacted primary particles to rearrange and form a single spherical particle. The coalescence of Ni nanoparticles is sensitive to the phase (molten or solid) of the nanoparticles.

Our calculation shows that a nanoparticle with a diameter less than 1.5 nm is liquid at 600 °C, even though its bulk melting point is 1450 °C (see Figure S8). The characteristic coalescence time for Ni nanoparticles was computed based on the phase of Ni nanoparticles. When the size of nanoparticles was less than 1.5 nm, and thus the liquid phase, a viscous flow mechanism, as shown in eq 6, was used to calculate the coalescence time[52]

$$\tau_l = \frac{\mu d_{eff}}{2\sigma_l} \tag{6}$$

DOI: 10.1021/acs.langmuir.7b02900
Langmuir 2018, 34, 585–594

where μ is the viscosity of the Ni nanoparticle, σ_l is the surface tension of Ni in the liquid state, d_{eff} is the effective diameter of the coalescing particle pair, which is $6V_p/a_p$, where V_p and a_p are the volume and the surface area of the coalescing particle pair, respectively. The data of all the properties employed can be found in the Supporting Information.

If Ni nanoparticles are in the solid phase, the coalescence time for Ni nanoparticles can be described with the following equation[53]

$$\tau_s = \frac{3k_B T_p N}{64\pi\sigma_s D_{eff}} \quad (7)$$

where T_p is the temperature of a particle pair undergoing coalescence, N is the number of atoms in the particle pair, σ_s is the surface tension of the solid Ni nanoparticle, and D_{eff} is the effective atomic diffusion coefficient in the particle pair. The property data are given in the Supporting Information.

Figure 9 shows the characteristic coalescence, coagulation, and residence time as a function of diameter. Interestingly, for nanoparticles with a diameter less than 1.5 nm, both coagulation and coalescence times are less than the residence time, which suggests that both coagulation and coalescence should be occurring during the early stages of growth. This result is consistent with the previous discussion that coagulation of nuclei occurs at the early stages of nanoparticle formation at 600 °C, leading to the decrease of the areal concentration of Ni nanoparticles (see Figure 8). However, solidification of Ni as seen by the rapid jump in the coalescence time above the residence time implies that any coagulation event would lead to an aggregate. However, aggregated particles are not observed, suggesting that the nanoparticles are not moving as independent entities in the polymer or else they would be forming agglomerates. It is more likely that as the nanoparticle moves, it carries with it a polymer layer which retards its diffusion rate.[54]

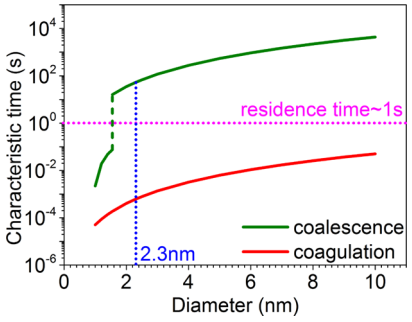

Figure 9. Characteristic sintering and coagulation time as a function of Ni nanoparticle diameter at 600 °C. The green dashed line represents the transition of the melting point of Ni nanoparticles.

Experimental particle size distributions (PSDs) are often used to deduce growth mechanisms.[55−57] It is well-known that the PSD for Brownian coagulation will approach an asymptotic (self-preserving) form regardless of the initial size distribution.[58] This self-preserving PSD can be approximated by a lognormal distribution function with a geometric SD of 1.44 for continuum regime.[59,60] The self-preserving PSD is written as

$$\frac{n(v)v}{N_\infty} = \frac{1}{3\sqrt{2\pi}\,\ln\sigma_g}\exp\left(\frac{-(\ln^2(v/v_g))}{18\ln^2\sigma_g}\right) \quad (8)$$

where v is the particle volume, $n(v)$ is the number concentration, N_∞ is the total number of particles, $v_g = \frac{1}{6}\pi d_g^3$ is the geometric number mean particle volume, d_g is the geometric number mean particle diameter, σ_g is the geometric SD of self-preserving PSD, 1.44. The scaled self-preserving PSD is plotted against the normalized particle diameter instead of normalized particle volume, v/v_g, which is shown in Figure 10.

On the other hand, if the growth of the ensemble is dominated by Ostwald ripening, the PSD is often approximated with the Lifshitz−Slyozov−Wagner (LSW) model.[61] An analytical expression of the PSD in the asymptote is given as[55,62]

$$f(\varphi) = A\varphi^2\left(\frac{3}{3+\varphi}\right)^{7/3}\left(\frac{1.5}{1.5-\varphi}\right)^{11/3}\exp\left(\frac{-\varphi}{1.5-\varphi}\right) \quad (9)$$

where φ is the ratio of the particle diameter to the average diameter and A is a function of time. There is a cutoff at φ = 1.5, above which $f(\varphi)$ becomes 0. Normalizing $f(\varphi)$ by the integral yields the famous PSD predicted by the LSW model. Term A does not affect the shape of normalized $f(\varphi)$.

The experimental PSD of Ni nanoparticles generated with different reaction temperatures and various metal salt to PVP ratios are shown in Figure 10. The self-preserving PSD for Brownian coagulation and PSDs predicted by the LSW model are also shown in Figure 10. Clearly, the self-preserving model provides a poor representation of the experimental PSD. The

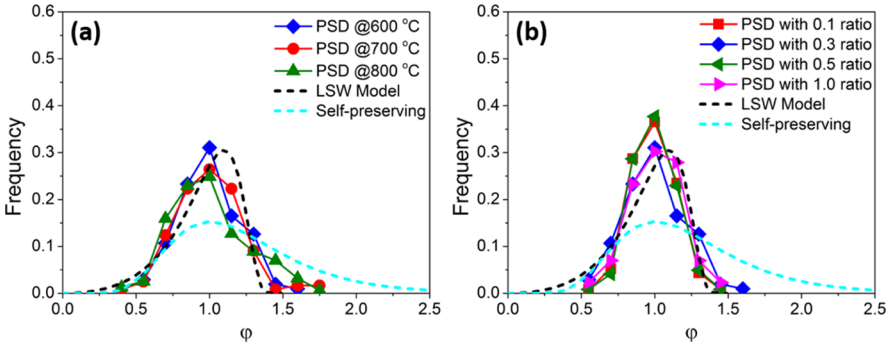

Figure 10. Scaled nanoparticle size distribution measured for three different reaction temperatures with a fixed metal salt to PVP ratio of 0.3 (a) and for four different metal salt to PVP ratios with a fixed reaction temperature of 600 °C (b). Dashed light blue line is the size distribution obtained for log-normally self-preserving size, and the dashed black line is the LSW size distribution.

DOI: 10.1021/acs.langmuir.7b02900
Langmuir 2018, 34, 585−594

peaks of all experimentally measured PSDs are much narrower than the log-normally self-preserving PSD. Even though some coagulation was observed for the samples treated at 800 °C and the corresponding PSD became a little bit broader, its PSD still does not reach the self-preserving PSD by coagulation. As shown in Table 2, the geometric SDs for all cases are smaller than 1.44, the self-preserving limit. The poor representation of the self-preserving coagulation model indicates that the coagulation is not a dominant growth mechanism. This result is consistent with our prior discussion that the polymer layer on the surface of the nanoparticles might hinder the coagulation between nanoparticles. The size distribution predicted by Ostwald ripening also seems to be a poor representation as the shape of the distribution is not correct. The experimental distributions are more symmetrical, whereas LSW is far more skewed to larger sizes. We may conclude that after an initial nucleation burst, growth is predominately by the surface addition of monomers and that coagulation only takes place at the highest temperatures and loadings explored.

Table 2. Geometric SDs σ for Ni Nanoparticles Generated at Different Conditions

metal salt to PVP ratio	σ_g	reaction temperature	σ_g
0.1	1.18	600 °C	1.18
0.3	1.23	700 °C	1.26
0.5	1.16	800 °C	1.31
1.0	1.22	self-preserving PSD	1.44

We schematically represent our best understanding of the experimental results in Figure 11. Initially, metal ions dispersed in a polymer particle (phase I) are rapidly reduced to metal atoms by hydrogen at the elevated temperature of 600 °C. This process is rapid compared to the residence time of 1 s. Studies have shown that diffusivity of gaseous molecules in a polymer matrix at elevated temperature is in the order of 10^4 cm^2/s;[41] thus, we should not be limited by the diffusion rate of H_2 molecules. We estimate the diffusion time for a 1 μm polymer droplet to be <5 μs. It has been found that the reduction of nickel oxides with a diameter of 10−20 μm by hydrogen is a first order reaction with a rate constant of 0.1 s^{-1} at 600 °C.[63] Therefore, the time for the half conversion of nickel oxides is in the order of 1 s.[63] However, this assumes that we first produce the oxide, which is a worst case scenario. Assuming the metal atoms were uniformly dispersed in the polymer melt, homogenous nucleation will create a large number of small cluster nuclei. Initial coagulation between nuclei may occur, but the primary growth mechanism appears to be, based on the morphological evidence, the surface addition of metal to existing nuclei. Isolated metal particles occur at temperatures sufficient to generate metal from the precursor, but not so high as to enable particles to have sufficient diffusion rates to coagulate to form aggregates (seen at higher temperatures), given that the coalescence time is relatively long. It is likely that the polymer melt retards coagulation growth by an add-layer of the polymer.

4. SUMMARY AND CONCLUSIONS

We demonstrate an aerosol single-drop reactor approach to grow and stabilize metal nanoclusters in a polymer matrix. The rapid thermal pulse given to the aerosol particles enables the formation of nuclei and growth, with subsequent rapid quenching to freeze in the structure. The size of metal nanoclusters can be controlled by adjusting the mass loading ratio of metal salt to polymer matrix and the temperature of the tubular reactor. On the basis of the experimental observation and quantitative analysis, we conclude that the growth is governed by nucleation and surface growth with little coagulation or Ostwald ripening. Finally, we note that this aerosol route is amenable to scale-up for large-scale production of nanoclusters that can either be used as is within the polymer or released by solvent extraction, depending on the application.

■ ASSOCIATED CONTENT

Supporting Information

The Supporting Information is available free of charge on the ACS Publications website at DOI: 10.1021/acs.langmuir.7b02900.

Stability of PVP molecules against heat treatment; component analysis of metal−polymer nanocomposites; scanning TEM, EDS mapping, and line scanning characterization for Ni-PVP-8k nanocomposite; and property data used for the characteristic time analysis (PDF)

■ AUTHOR INFORMATION

Corresponding Author

*E-mail: mrz@umd.edu.

ORCID

Tao Wu: 0000-0003-3704-275X

Michael R. Zachariah: 0000-0002-4115-3324

Notes

The authors declare no competing financial interest.

■ ACKNOWLEDGMENTS

Support for this works comes from an ONR-MURI grant. We also acknowledge the support of the Maryland Nanocenter and its AIM lab.

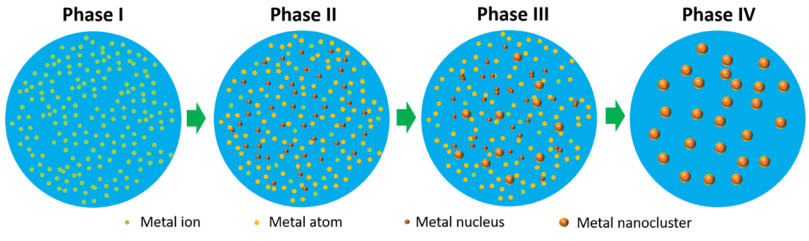

Figure 11. Schematic of the nucleation and growth of metal nanoparticles in the polymer melt at 600 °C.

DOI: 10.1021/acs.langmuir.7b02900
Langmuir 2018, 34, 585−594

REFERENCES

(1) Olson, J.; Dominguez-Medina, S.; Hoggard, A.; Wang, L.-Y.; Chang, W.-S.; Link, S. Optical characterization of single plasmonic nanoparticles. *Chem. Soc. Rev.* **2015**, *44*, 40−57.

(2) Boisselier, E.; Astruc, D. Gold nanoparticles in nanomedicine: preparations, imaging, diagnostics, therapies and toxicity. *Chem. Soc. Rev.* **2009**, *38*, 1759−1782.

(3) Lu, A.-H.; Salabas, E. L.; Schüth, F. Magnetic nanoparticles: synthesis, protection, functionalization, and application. *Angew. Chem., Int. Ed.* **2007**, *46*, 1222−1244.

(4) Ozbay, E. Plasmonics: merging photonics and electronics at nanoscale dimensions. *Science* **2006**, *311*, 189−193.

(5) Choi, K. M.; Na, K.; Somorjai, G. A.; Yaghi, O. M. Chemical environment control and enhanced catalytic performance of platinum nanoparticles embedded in nanocrystalline metal−organic frameworks. *J. Am. Chem. Soc.* **2015**, *137*, 7810−7816.

(6) Zhang, J.; Xu, S.; Kumacheva, E. Polymer microgels: reactors for semiconductor, metal, and magnetic nanoparticles. *J. Am. Chem. Soc.* **2004**, *126*, 7908−7914.

(7) Ramesh, G. V.; Porel, S.; Radhakrishnan, T. P. Polymer thin films embedded with in situ grown metal nanoparticles. *Chem. Soc. Rev.* **2009**, *38*, 2646−2656.

(8) Faupel, F.; Zaporojtchenko, V.; Strunskus, T.; Elbahri, M. Metal-polymer nanocomposites for functional applications. *Adv. Eng. Mater.* **2010**, *12*, 1177−1190.

(9) Firestone, M. A.; Hayden, S. C.; Huber, D. L. Greater than the sum: Synergy and emergent properties in nanoparticle−polymer composites. *MRS Bull.* **2015**, *40*, 760−767.

(10) Kutvonen, A.; Rossi, G.; Puisto, S. R.; Rostedt, N. K. J.; Ala-Nissila, T. Influence of nanoparticle size, loading, and shape on the mechanical properties of polymer nanocomposites. *J. Chem. Phys.* **2012**, *137*, 214901.

(11) Zaragoza, J.; Babhadiashar, N.; O'Brien, V.; Chang, A.; Blanco, M.; Zabalegui, A.; Lee, H.; Asuri, P. Experimental investigation of mechanical and thermal properties of silica nanoparticle-reinforced poly(acrylamide) nanocomposite hydrogels. *PLoS One* **2015**, *10*, No. e0136293.

(12) Sygletou, M.; Tzourmpakis, P.; Petridis, C.; Konios, D.; Fotakis, C.; Kymakis, E.; Stratakis, E. Laser induced nucleation of plasmonic nanoparticles on two-dimensional nanosheets for organic photovoltaics. *J. Mater. Chem. A* **2016**, *4*, 1020−1027.

(13) Wu, H.; Yu, G.; Pan, L.; Liu, N.; McDowell, M. T.; Bao, Z.; Cui, Y. Stable Li-ion battery anodes by in-situ polymerization of conducting hydrogel to conformally coat silicon nanoparticles. *Nat. Commun.* **2013**, *4*, 1943.

(14) Porta, M.; Nguyen, M. T.; Ishida, Y.; Yonezawa, T. Highly stable and blue-emitting copper nanocluster dispersion prepared by magnetron sputtering over liquid polymer matrix. *RSC Adv.* **2016**, *6*, 105030−105034.

(15) Slistan-Grijalva, A.; Herrera-Urbina, R.; Rivas-Silva, J. F.; Ávalos-Borja, M.; Castillón-Barraza, F.; Posada-Amarillas, A. Synthesis of silver nanoparticles in a polyvinylpyrrolidone (PVP) paste, and their optical properties in a film and in ethylene glycol. *Mater. Res. Bull.* **2008**, *43*, 90−96.

(16) Porel, S.; Singh, S.; Harsha, S. S.; Rao, D. N.; Radhakrishnan, T. P. Nanoparticle-embedded polymer: in situ synthesis, free-standing films with highly monodisperse silver nanoparticles and optical limiting. *Chem. Mater.* **2005**, *17*, 9−12.

(17) Jin, W.-J.; Lee, H. K.; Jeong, E. H.; Park, W. H.; Youk, J. H. Preparation of Polymer Nanofibers Containing Silver Nanoparticles by Using Poly(N-vinylpyrrolidone). *Macromol. Rapid Commun.* **2005**, *26*, 1903−1907.

(18) Zhang, J.; Xu, S.; Kumacheva, E. Photogeneration of fluorescent silver nanoclusters in polymer microgels. *Adv. Mater.* **2005**, *17*, 2336−2340.

(19) Ramesh, G. V.; Sreedhar, B.; Radhakrishnan, T. P. Real time monitoring of the in situ growth of silver nanoparticles in a polymer film under ambient conditions. *Phys. Chem. Chem. Phys.* **2009**, *11*, 10059−10063.

(20) Hariprasad, E.; Radhakrishnan, T. P. In situ fabricated polymer−silver nanocomposite thin film as an inexpensive and efficient substrate for surface-enhanced Raman scattering. *Langmuir* **2013**, *29*, 13050−13057.

(21) Motl, N. E.; Mann, A. K. P.; Skrabalak, S. E. Aerosol-assisted synthesis and assembly of nanoscale building blocks. *J. Mater. Chem. A* **2013**, *1*, 5193−5202.

(22) Athanassiou, E. K.; Grass, R. N.; Stark, W. J. Chemical aerosol engineering as a novel tool for material science: from oxides to salt and metal nanoparticles. *Aerosol Sci. Technol.* **2010**, *44*, 161−172.

(23) Bang, J. H.; Suslick, K. S. Applications of ultrasound to the synthesis of nanostructured materials. *Adv. Mater.* **2010**, *22*, 1039−1059.

(24) Shatrova, N.; Yudin, A.; Levina, V.; Dzidziguri, E.; Kuznetsov, D.; Perov, N.; Issi, J.-P. Elaboration, characterization and magnetic properties of cobalt nanoparticles synthesized by ultrasonic spray pyrolysis followed by hydrogen reduction. *Mater. Res. Bull.* **2017**, *86*, 80−87.

(25) Liang, Y.; Hou, H.; Yang, Y.; Glicksman, H.; Ehrman, S. Conductive One- and Two-Dimensional Structures Fabricated Using Oxidation-Resistant Cu−Sn Particles. *ACS Appl. Mater. Interfaces* **2017**, *9*, 34587−34591.

(26) Wu, C.; Lee, D.; Zachariah, M. R. Aerosol-based self-assembly of nanoparticles into solid or hollow mesospheres. *Langmuir* **2010**, *26*, 4327−4330.

(27) Kim, S. H.; Liu, B. Y. H.; Zachariah, M. R. Ultrahigh Surface Area Nanoporous Silica Particles via an Aero-Sol−Gel Process. *Langmuir* **2004**, *20*, 2523−2526.

(28) Firmansyah, D. A.; Kim, T.; Kim, S.; Sullivan, K.; Zachariah, M. R.; Lee, D. Crystalline phase reduction of cuprous oxide (Cu2O) nanoparticles accompanied by a morphology change during ethanol-assisted spray pyrolysis. *Langmuir* **2009**, *25*, 7063−7071.

(29) Atkinson, J. D.; Fortunato, M. E.; Dastgheib, S. A.; Rostam-Abadi, M.; Rood, M. J.; Suslick, K. S. Synthesis and characterization of iron-impregnated porous carbon spheres prepared by ultrasonic spray pyrolysis. *Carbon* **2011**, *49*, 587−598.

(30) Suh, W. H.; Suslick, K. S. Magnetic and porous nanospheres from ultrasonic spray pyrolysis. *J. Am. Chem. Soc.* **2005**, *127*, 12007−12010.

(31) Chen, Y.; Guo, F.; Jachak, A.; Kim, S.-P.; Datta, D.; Liu, J.; Kulaots, I.; Vaslet, C.; Jang, H. D.; Huang, J.; Kane, A.; Shenoy, V. B.; Hurt, R. H. Aerosol synthesis of cargo-filled graphene nanosacks. *Nano Lett.* **2012**, *12*, 1996−2002.

(32) Xia, B.; Lenggoro, I. W.; Okuyama, K. Novel Route to Nanoparticle Synthesis by Salt-Assisted Aerosol Decomposition. *Adv. Mater.* **2001**, *13*, 1579−1582.

(33) Didenko, Y. T.; Suslick, K. S. Chemical aerosol flow synthesis of semiconductor nanoparticles. *J. Am. Chem. Soc.* **2005**, *127*, 12196−12197.

(34) Lee, K. H.; Rah, S. C.; Kim, S.-G. Formation of monodisperse silver nanoparticles in poly(vinylpyrrollidone) matrix using spray pyrolysis. *J. Sol-Gel Sci. Technol.* **2008**, *45*, 187−193.

(35) Seo, J. Y.; Kang, H. W.; Jung, D. S.; Lee, H. M.; Park, S. B. One-step synthesis of copper nanoparticles embedded in carbon composites. *Mater. Res. Bull.* **2013**, *48*, 1484−1489.

(36) Wang, X.; Zhou, W.; DeLisio, J. B.; Egan, G. C.; Zachariah, M. R. Doped δ-bismuth oxides to investigate oxygen ion transport as a metric for condensed phase thermite ignition. *Phys. Chem. Chem. Phys.* **2017**, *19*, 12749−12758.

(37) Gürmen, S.; Stopić, S.; Friedrich, B. Synthesis of nanosized spherical cobalt powder by ultrasonic spray pyrolysis. *Mater. Res. Bull.* **2006**, *41*, 1882−1890.

(38) Jung, K. Y.; Lee, J. H.; Koo, H. Y.; Kang, Y. C.; Park, S. B. Preparation of solid nickel nanoparticles by large-scale spray pyrolysis of Ni(NO3)2 6H2O precursor: Effect of temperature and nickel acetate on the particle morphology. *Mater. Sci. Eng. B* **2007**, *137*, 10−19.

DOI: 10.1021/acs.langmuir.7b02900
Langmuir 2018, 34, 585−594

(39) Majumdar, D.; Shefelbine, T. A.; Kodas, T. T.; Glicksman, H. D. Copper (I) oxide powder generation by spray pyrolysis. *J. Mater. Res.* **1996**, *11*, 2861−2868.
(40) Tannenbaum, R.; Zubris, M.; Goldberg, E. P.; Reich, S.; Dan, N. Polymer-directed nanocluster synthesis: control of particle size and morphology. *Macromolecules* **2005**, *38*, 4254−4259.
(41) Faupel, F.; Willecke, R.; Thran, A. Diffusion of metals in polymers. *Mater. Sci. Eng., R* **1998**, *22*, 1−55.
(42) Brockner, W.; Ehrhardt, C.; Gjikaj, M. Thermal decomposition of nickel nitrate hexahydrate, Ni(NO3)2 6H2O, in comparison to Co(NO3)2 6H2O and Ca(NO3)2 4H2O. *Thermochim. Acta* **2007**, *456*, 64−68.
(43) Kane, R. S.; Cohen, R. E.; Silbey, R. Semiconductor nanocluster growth within polymer films. *Langmuir* **1999**, *15*, 39−43.
(44) Thanh, N. T. K.; Maclean, N.; Mahiddine, S. Mechanisms of nucleation and growth of nanoparticles in solution. *Chem. Rev.* **2014**, *114*, 7610−7630.
(45) Park, J.; Joo, J.; Kwon, S. G.; Jang, Y.; Hyeon, T. Synthesis of monodisperse spherical nanocrystals. *Angew. Chem., Int. Ed.* **2007**, *46*, 4630−4660.
(46) Dan, N.; Zubris, M.; Tannenbaum, R. Effect of polymeric media on the kinetics of nanocluster nucleation and growth. *Macromolecules* **2005**, *38*, 9243−9250.
(47) Einstein, A. Über die von der molekularkinetischen Theorie der Wärme geforderte Bewegung von in ruhenden Flüssigkeiten suspendierten Teilchen. *Ann. Phys.* **1905**, *322*, 549−560.
(48) Rubinstein, M.; Colby, R. H. *Polymer Physics*; Oxford University: New York, 2003.
(49) Gupta, S. S.; Meena, A.; Parikh, T.; Serajuddin, A. Investigation of thermal and viscoelastic properties of polymers relevant to hot melt extrusion-I: Polyvinylpyrrolidone and related polymers. *J. Excipients Food Chem.* **2014**, *5*, 32−45.
(50) Masuko, T.; Magill, J. H. A Comprehensive Expression for Temperature Dependence of Liquid Viscosity. *Nippon Reoroji Gakkaishi* **1988**, *16*, 22−26.
(51) Friedlander, S. K. *Smoke, Dust, and Haze: Fundamentals of Aerosol Dynamics*; Topics in Chemical Engineering; Oxford University Press: New York, 2000.
(52) Mukherjee, D.; Sonwane, C. G.; Zachariah, M. R. Kinetic Monte Carlo simulation of the effect of coalescence energy release on the size and shape evolution of nanoparticles grown as an aerosol. *J. Chem. Phys.* **2003**, *119*, 3391−3404.
(53) Wu, M. K.; Windeler, R. S.; Steiner, C. K. R.; Börs, T.; Friedlander, S. K. Controlled synthesis of nanosized particles by aerosol processes. *Aerosol Sci. Technol.* **1993**, *19*, 527−548.
(54) Griffin, P. J.; Bocharova, V.; Middleton, L. R.; Composto, R. J.; Clarke, N.; Schweizer, K. S.; Winey, K. I. Influence of the bound polymer layer on nanoparticle diffusion in polymer melts. *ACS Macro Lett.* **2016**, *5*, 1141−1145.
(55) Woehl, T. J.; Park, C.; Evans, J. E.; Arslan, I.; Ristenpart, W. D.; Browning, N. D. Direct observation of aggregative nanoparticle growth: Kinetic modeling of the size distribution and growth rate. *Nano Lett.* **2014**, *14*, 373−378.
(56) Sholl, D. S.; Skodje, R. T. Late-stage coarsening of adlayers by dynamic cluster coalescence. *Phys. A* **1996**, *231*, 631−647.
(57) Simonsen, S. B.; Chorkendorff, I.; Dahl, S.; Skoglundh, M.; Sehested, J.; Helveg, S. Direct observations of oxygen-induced platinum nanoparticle ripening studied by in situ TEM. *J. Am. Chem. Soc.* **2010**, *132*, 7968−7975.
(58) Friedlander, S. K.; Wang, C. S. The self-preserving particle size distribution for coagulation by Brownian motion. *J. Colloid Interface Sci.* **1966**, *22*, 126−132.
(59) Lee, K. W.; Chen, J.; Gieseke, J. A. Log-normally preserving size distribution for Brownian coagulation in the free-molecule regime. *Aerosol Sci. Technol.* **1984**, *3*, 53−62.
(60) Lee, K. W. Change of particle size distribution during Brownian coagulation. *J. Colloid Interface Sci.* **1983**, *92*, 315−325.
(61) Lifshitz, I. M.; Slyozov, V. V. The kinetics of precipitation from supersaturated solid solutions. *J. Phys. Chem. Solids* **1961**, *19*, 35−50.
(62) Wong, E. M.; Bonevich, J. E.; Searson, P. C. Growth kinetics of nanocrystalline ZnO particles from colloidal suspensions. *J. Phys. Chem. B* **1998**, *102*, 7770−7775.
(63) Richardson, J. T.; Scates, R.; Twigg, M. V. X-ray diffraction study of nickel oxide reduction by hydrogen. *Appl. Catal., A* **2003**, *246*, 137−150.

DOI: 10.1021/acs.langmuir.7b02900
Langmuir 2018, 34, 585−594